AIAA 03–4005

Active Control of Separation From the Flap of a Supercritical Airfoil

LaTunia Pack Melton and Chung-Sheng Yao
Flow Physics and Control Branch
NASA Langley Research Center, Hampton, VA 23681

Avi Seifert
Tel-Aviv University, Ramat-Aviv 69978, ISRAEL

33rd AIAA Fluid Dynamics Conference
June 23–26, 2003/Orlando, FL

Active Control of Separation From the Flap of a Supercritical Airfoil

LaTunia Pack Melton* and Chung-Sheng Yao†
Flow Physics and Control Branch
NASA Langley Research Center, Hampton, VA 23681
Avi Seifert ‡
Tel-Aviv University, Ramat-Aviv 69978, ISRAEL

Active flow control in the form of periodic zero-mass-flux excitation was applied at several regions on the leading edge and trailing edge flaps of a simplified high-lift system to delay flow separation. The NASA Energy Efficient Transport (EET) supercritical airfoil was equipped with a 15% chord simply hinged leading edge flap and a 25% chord simply hinged trailing edge flap. Detailed flow features were measured in an attempt to identify optimal actuator placement. The measurements included steady and unsteady model and tunnel wall pressures, wake surveys, arrays of surface hot-films, flow visualization, and particle image velocimetry (PIV). The current paper describes the application of active separation control at several locations on the deflected trailing edge flap. High frequency ($F^+ \approx 10$) and low frequency amplitude modulation ($F^+_{AM} \approx 1$) of the high frequency excitation were used for control. Preliminary efforts to combine leading and trailing edge flap excitations are also reported.

Nomenclature

c	model chord
$< c_\mu >$	oscillatory excitation momentum coefficient, $\equiv < J' > /cq$
C_{dp}	pressure drag coefficient
C_D	total drag
C_L	lift coefficient
$C_{L,max}$	maximum lift coefficient
C_p	pressure coefficient, $\equiv (P - P_s)/q$
$C_{p,min}$	minimum pressure coefficient
f	oscillation frequency, Hz
F^+	reduced frequency, $\equiv (f x_{sp})/U_{\inf}$
h	slot height or width
J'	oscillatory momentum at slot exit, $\equiv \rho h u_j'^2$
M	Mach number
P	pressure
P_s	static pressure
q	freestream dynamic pressure,$\equiv 1/2\rho U\infty^2$
Re_c	chord Reynolds number, $\equiv U_\infty c/\nu$
x_{sp}	distance from actuator to trailing edge
T	temperature
U, u	average and fluctuating streamwise velocity
x/c	normalized streamwise location
z	spanwise location
α	angle of attack
δ_f	TE flap deflection
δ_s	LE flap deflection
ν	kinematic viscosity
ρ	density

Abbreviations

AFC	active flow control
AM	amplitude modulation
BL	boundary layer
LE	leading edge
TE	trailing edge
VSF	vortex shedding frequency

Subscripts

b	baseline flow conditions
c	cavity
d	de-rectified hot-wire data
j	conditions at excitation slot
N	normalized according to text
R	reattachment
S	separation
∞	freestream conditions

Superscript

$'$	root mean square of fluctuating value

*Member of AIAA, l.g.pack@larc.nasa.gov
†c.s.yao@larc.nasa.gov
‡Associate Fellow, AIAA, seifert@eng.tau.ac.il, Senior lecturer, Dept. of Fluid Mechanics and Heat Transfer, Faculty of Engineering and visiting scientist National Institute of Aerospace, Hampton, VA

1 Introduction

NUMEROUS experiments at both low[1] and high[2,3] Reynolds numbers have shown that periodic excitation is effective as well as efficient in terms

of momentum at controlling separation. This information combined with that of a system study[4] indicating the possibility of significant payoffs such as net airplane cost, weight, and cruise drag reductions has lead to the application of active separation control to a simplified high-lift system. The purpose of the current investigation is to explore ways to simplify current multi-element high-lift airfoils[5] that use slots and the Fowler effect to generate high lift. The chosen design completely eliminates hinges and positioning actuators that are external to the airfoil contour as well as passive slots for energizing the boundary layer. All hinges and positioning actuators are internal, and thus reduce parasite drag at cruise. The leading edge (LE) flap is used to increase $C_{L,max}$ due to increased circulation and prevention of laminar leading edge separation. Zero-mass-flux periodic excitation, directed downstream at a shallow angle to the local surface, is applied at locations that are prone to separation, i.e. the LE and trailing edge (TE) flap shoulders.

Flow control research using steady momentum transfer on a high–lift system dates back to the 1930's.[6] Additional interest was spurred in the 1950's by the use of the gas turbine engine. The research showed that separation could be controlled effectively using steady momentum but that the momentum requirement was very large.[6] The use of periodic excitation for separation control on the simply hinged high-lift system should reduce the momentum requirements compared to that of steady excitation. In addition, research using pulsed excitation has also shown that the momentum requirements can be reduced further by varying the duty cycle of the excitation.[7]

The results obtained when applying periodic excitation at the LE flap shoulder of this airfoil were reported in a previous publication.[8] High frequency periodic excitation, typical of the piezoelectric actuators currently used, was applied at the LE flap shoulder, and delayed stall and increased $C_{L,max}$ by 10-15%, at low TE flap deflections. It was shown that low frequency amplitude modulation could be used to achieve similar benefits in aerodynamic performance and required 50% -70% less $< c_\mu >$. In this paper. the effect of introducing periodic excitation on the TE flap upstream of the turbulent boundary layer separation location is examined.

2 Experiment

Details about the wind tunnel and instrumentation can be found in Ref. 8. Included here are details about the model and actuator used for controlling flow separation on the TE flap.

2.1 Simplified High–Lift Model

The simplified high lift version of the NASA EET airfoil[5] was designed in a modular manner so that zero-net mass flux actuators could replace solid regions in the model near the LE and TE flap shoulders (Fig. 1(a)). The 406.4 mm chord model has a 15% chord LE flap that can be deflected from 0 to -30 deg and a 25% chord trailing edge flap that can be deflected from 0 to 60 deg. Angle of attack settings for the airfoil and the two flaps were automated and closed-loop computer controlled. The model has 78 streamwise static pressure taps located at mid span and two rows of 18 spanwise static pressure taps spaced 50.8 mm apart located at x/c = 0.35 and x/c = 0.94. In addition to the static pressure taps, there are nine unsteady pressure transducers on the model surface and at least one unsteady pressure transducer embedded in each actuator cavity for monitoring the pressure fluctuations produced by the actuator and correlating the wind tunnel experiment with the bench-top actuator calibration tests.

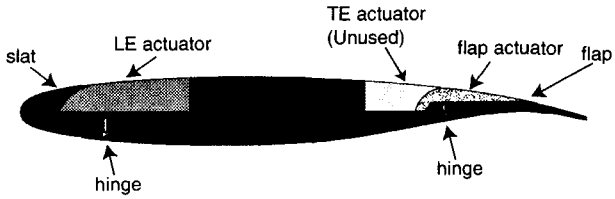

a) Actuator regions of EET model.

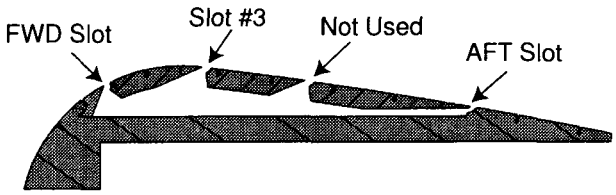

b) Flap actuator cross–section.

Fig. 1 Modified EET model

2.2 TE Flap Actuator

An internal Piezo-electric actuator was used on the TE flap (Figs. 1). The TE flap actuator, with its four alternative excitation slots, all inclined at about 30° to the surface and facing downstream, is shown in Figure 1(b). The three upstream slots are 0.635 mm wide, and the aft slot is 0.51 mm wide. The x/c locations for the TE flap actuator slots ($\delta_f = 0^o$) are given in Table 1.

Table 1 Flap actuator slot locations

Slot	x/c location at $\delta_f = 0^o$
FWD	0.725
#3	0.757
Not Used	0.790
AFT	0.845

The three forward slots are segmented and the aft slot is continuous. The three forward slots each have 19 segments that are 0.051m in length . A comprehensive bench-top calibration, using a single hot wire that

was traversed along the span of each slot with all other slots sealed, was performed on the TE flap actuator prior to installation in the tunnel, and unsteady pressures were measured in the actuators cavity to monitor its operation during the calibration and while in the tunnel. The flap actuator was operated at its resonant frequency (1 kHz ± 0.3 kHz, depending on the slot used) using a pure sine wave and also with an amplitude modulation (AM) at frequencies lower by an order of magnitude than the actuator's resonant frequency. Only one slot was active during each experiment. The three forward slots were sealed using a water-soluble filler to minimize surface discontinuities, and 0.051 mm thick, 12.7 mm wide kapton tape was used on the aft slot.

2.3 PIV Set-Up

Two-dimensional digital particle image velocimetry (PIV) was used to measure the instantaneous flow fields phase synchronized with the flap actuator cycle. The PIV system includes two 1K x 1K cameras installed side by side with 105 mm Macro lens. The fields of view from the two cameras were overlapped to capture the entire flap region. The width of the measurement plane was about 120 mm. A non–rectangular grid was used with a minimum resolution of 24 x 24 pixels. The maximum overlap between adjacent interrogation regions was 50%. Smoke, introduced upstream of the wind tunnel contraction, was used for seeding. Dual Nd-Yag lasers were used to illuminate a light sheet, placed about 50 mm off the model centerline.

2.4 Experimental Uncertainty

The α's presented are accurate to within $\pm 0.03^o$. The LE and TE flap deflection angles are accurate to within $\pm 0.25^o$, $< c_\mu >$ is accurate to within 20% (partly due to slot width uncertainty of ±0.08 mm and partly due to calibration uncertainties such as wire location and ±2% uncertainty in hot-wire velocity measurements), and Re_c is accurate to within 3%. The uncertainties of the airfoil integral parameters are listed in Table 2 (in absolute values and related to flow conditions).

Table 2 Uncertainty of Airfoil integral parameters

Parameter	Fully attached	Stalled	Controlled
C_L	0.01	0.04	0.02
C_{dp}	0.002	0.004	0.003
C_D	0.002	0.008	0.006

The large uncertainty in the total drag, C_D, is due to the extrapolation of the wake data for some of the high lift configurations of the airfoil, to wind tunnel interference, and to uncertainty about wind tunnel static pressure and wake rake location. It should be noted that the integral parameters in this paper were not corrected for the significant tunnel wall interference present in the BART facility for the model size used; however, the relative improvement in performance is believed to be conservative.

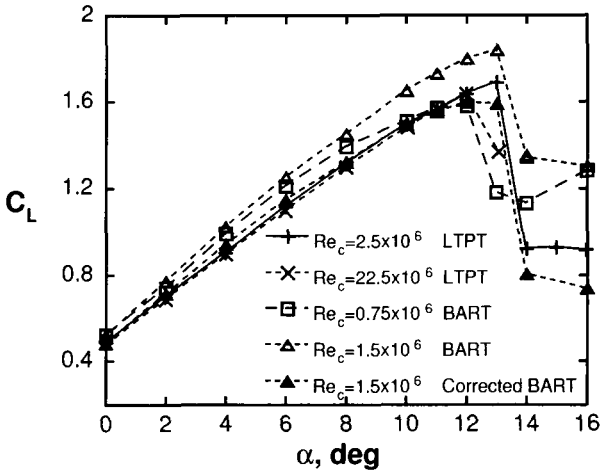

a) EET results from the BART and LTPT facilities at a range of Reynolds Numbers. $Re_c = 0.75x10^6, \delta_s = \delta_f = 0^o$.

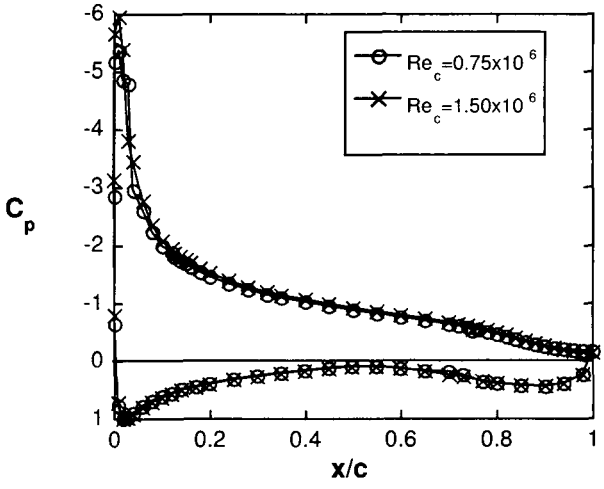

b) Airfoil pressure distributions, $\alpha = 8^o$, $\delta_s = \delta_f = 0^o$.

Fig. 2 EET cruise configuration Reynolds number comparison

2.5 Test Conditions (flow and geometry)

Most of the experiments using the TE flap were conducted at incompressible values of Re_c ranging from 0.24 x 10^6 to 0.75 x 10^6. The flap deflection was varied from $\delta_f = 0^o$ to 60^o, and δ_s was between 0^o and -30^o.

3 Results

3.1 Baseline Flow

3.1.1 Reynolds Number Effect

The baseline (no control) performance of the airfoil is discussed in Reference 8. Some of the baseline data is repeated and discussed here for completeness. The

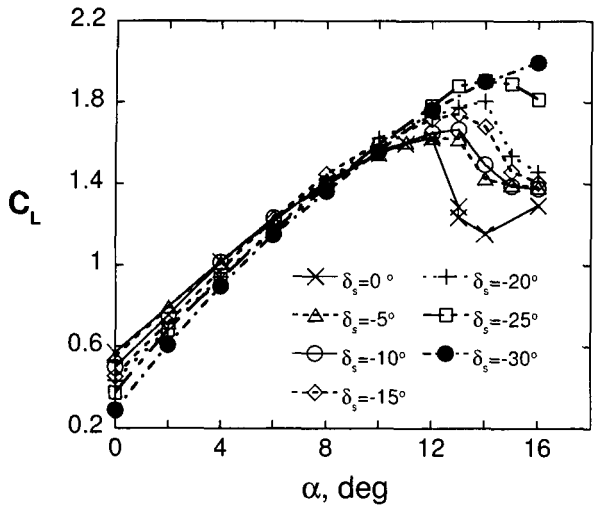

Fig. 3 Lift of the EET airfoil at different slat deflections. $Re_c = 0.75x10^6$, $\delta_f = 0^o$

baseline cruise configuration of the airfoil was tested and compared to previous tests of the same airfoil at a different facility and a different range of Mach and Reynolds numbers.[5] The data were acquired with the original airfoil contour, before any actuator slots were present. The lighter color regions shown in Figure 1(a) indicate alternative actuator locations. The highest available Re_c at BART, $1.5x10^6$, is lower than the lowest Re_c tested in the Low Turbulence Pressure Tunnel (LTPT), $2.5x10^6$. Figure 2(a) presents the lift data of the current airfoil versus the data of Lin.[9] The lift data indicate that, as expected, significant wall interference exists in the present BART set-up. Conventional wind tunnel walls interference and wake blockage corrections[10] were applied to the data, and the corrected BART lift (for $Re_c = 1.5x10^6$) is in very good agreement with the LTPT data (for $Re_c = 2.5x10^6$) for the cruise configuration. Weak Re_c effects such as increased lift at low α (due to a laminar separation bubble as shown in Fig. 2(b)) and earlier stall (due to a thicker BL) can be seen. Overall however, the reproduction of the LTPT data is satisfactory. Uncorrected lift data measured at BART at $Re_c = 0.75x10^6$ is also shown for comparison and is in good agreement with the higher Re_c data from BART for $Re_c = 1.5x10^6$. Besides stronger Re_c effects (shown for instance in the C_p of Fig. 2(b)), the three data sets are in reasonable agreement. Most of the data to be presented in this paper are for $Re_c = 0.24x10^6$ to $Re_c = 0.75x10^6$, and attention is paid that *turbulent* separation would always be considered, minimizing low Re_c effects. It is expected that wall interference will have a larger influence on the flow as the lift and drag increase, due to slat and flap deflections for the high lift configuration. However, the lift increment and especially the drag reduction with active separation control are expected to be conservative since tunnel interference, at least the wake blockage effect of it, will be reduced because the drag will decrease. Moreover, floor and ceiling pressures were acquired at all flow conditions to assist future data reduction and comparison to CFD, taking into account the tunnel walls.

3.1.2 Baseline-LE Flap Deflection

The purpose of deflecting the LE flap was to eliminate the possibility of LE separation that supercritical airfoils are notoriously known for due to the low radius of curvature of the LE.[11] Figure 3 demonstrates the effect of deflecting the LE flap on the lifting performance of the baseline airfoil at a fixed TE flap deflection angle of 0^o. The main effect of the LE flap deflection is to delay stall to a larger incidence and therefore increase the maximum lift generated by the airfoil. The stall is also milder at larger LE flap deflections, alleviating the abrupt stall shown for a LE flap deflection of zero. A secondary effect is a somewhat lower lift at low incidence and increased $d(C_L)/d(\alpha)$, in agreement with the progressively more cambered airfoil. The -30^o LE flap deflection case does not stall in the available range of α's, presumably due to tunnel interference, and therefore will not be considered. Overall, the LE flap has little effect on the pre-stall lifting performance of the airfoil.

3.1.3 Baseline-TE Flap Deflection

In application, it will be required to consider both LE and TE flap deflections for typical landing and to a lower extent for take-off. Figure 4(a) shows the lift data for increasing TE flap deflection at $Re_c = 0.75x10^6$. The typical TE flap effect[12] is shown where the lift is increased over the entire α range as the TE flap is deflected. Figure 4(b) presents the lift versus form–drag data, showing the TE flap effect as well. From the lift versus form–drag data, it is evident that the flapped airfoil behaves as a cambered airfoil up to a TE flap deflection of 10^o to 15^o, where the lift slope decreases with the incidence due to developing TE separation (Fig. 4(a)). At a TE flap deflection angle of 15^o, the TE flap upper surface is separated from the TE flap shoulder, causing a significant drag increase (Fig. 4(b)) and a constant lift slope (Fig. 4(a)) prior to stall that occurs at progressively smaller incidence as the TE flap deflection angle increases (Fig. 4(a)). This abrupt lift reduction occurs because separation abruptly shifts from the TE flap shoulder to the LE.

Figure 4(c) shows the maximum lift of the flapped airfoil at zero slat deflection and compares it with the corrected maximum lift according to Reference 11, taking the form drag for the wake blockage corrections, as it is not practical to measure wake drag at these highly unsteady separated flow conditions. The corrected flapped airfoil lift data shows that significant tunnel interference exists, and, as expected, the value of $d(C_L)/d(\delta_f)$ decreases significantly for $\delta_f > 7.5^o$.

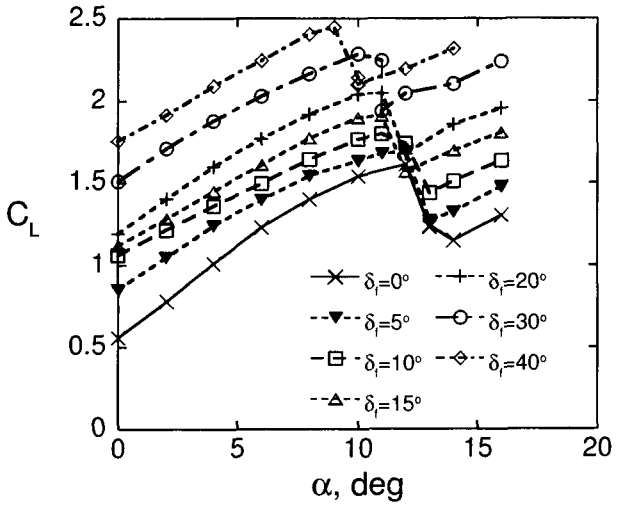

a) Lift vs. α at different flap deflections.

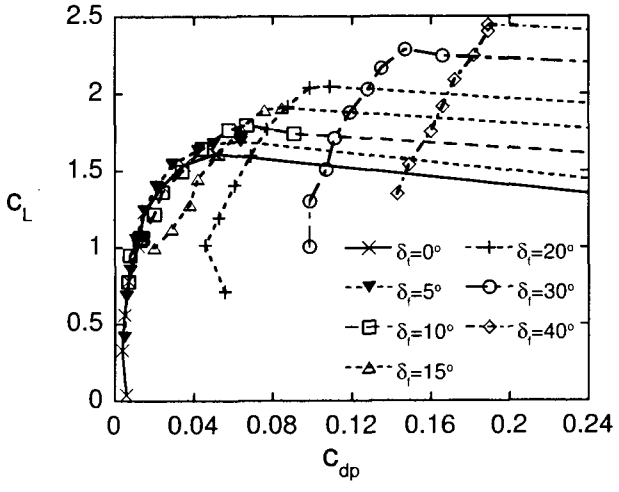

b) Lift vs. form drag at different flap deflections

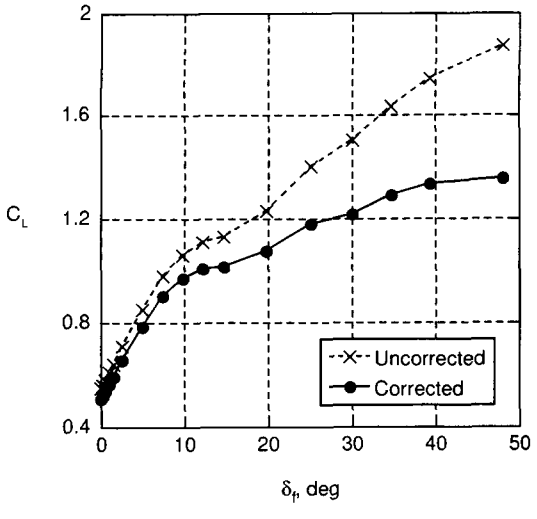

c) Corrected and Uncorrected lift vs. δ_f.

Fig. 4 Effect of flap deflection angle on airfoil integral parameters, $Re_c = 0.75x10^6, \delta_s = 0°$.

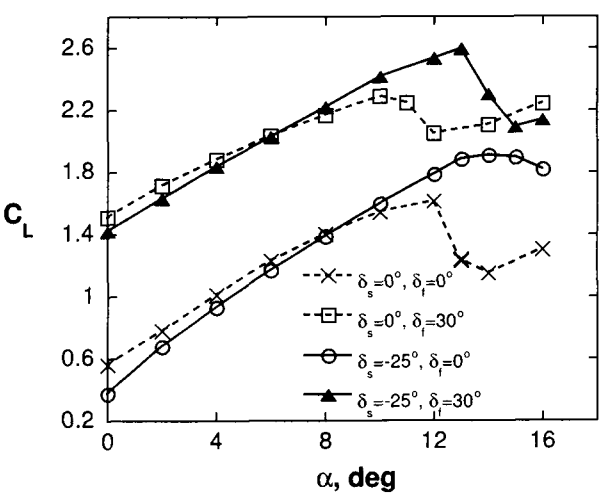

Fig. 5 Lift coefficients of the EET airfoil at different high lift configurations as tested in BART at $Re_c = 0.75x10^6$.

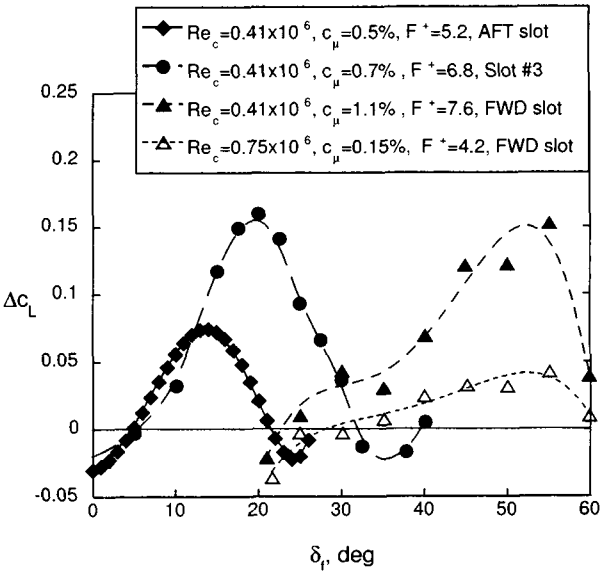

Fig. 6 Lift increment vs flap deflection angle for different slot locations (shown in Fig. 1(b)). $\alpha = 0°$, $\delta_s = 0°$. (Note that AFT slot data are from curve fits of the controlled and baseline data)

Negligible lift increments are obtained for TE flap deflections larger than $35°$. However, this could be altered if high frequency periodic excitation would be provided to increase the suction level at the TE flap shoulder.

3.1.4 Baseline-LE and TE Flap Deflection

A candidate flow condition ($\delta_s = -25°$ and $\delta_f = 30°$) for a landing configuration is shown in Figure 5. The data presented in this figure include the cruise configuration, LE flap deflection of $-25°$ at zero TE flap deflection (showing delayed and milder stall), TE flap deflection of $30°$ at zero LE flap deflection (show-

ing increased lift and earlier, more abrupt stall), and a combination of LE flap deflection of -25^o and TE flap deflection of 30^o. The lift data for the latter configuration show that the LE flap effect is almost linearly added to the TE flap effect and its stall milding capability is maintained even at a TE flap deflection of 30^o. The challenge is now to apply periodic excitation on both the LE and TE flap shoulders, and to delay BL separation at both locations, allowing larger LE and TE flap deflections with a resulting enhanced lift.

3.2 Effects of the Active TE Flap Slot Location

A summary of the major findings with regard to the optimal locations for the introduction of periodic excitation, keeping in mind that the aim is increasing the effectiveness of the TE flap, is given in Figure 6 for $\alpha = 0^o$. In all cases considered, the separating BL was turbulent. The aft slot, located at $x/c = 0.845$ ($\delta_f = 0^o$), becomes effective for $\delta_f > 5^o$, reaches optimal performance at $\delta_f = 12^o$, and loses its effectiveness at $\delta_f > 20^o$, where the separation point moves upstream of the aft slot. Slot #3, situated roughly 9%c upstream of the aft slot, starts being effective at $\delta_f \approx 10^o$, reaches it peak performance at $\delta_f \approx 20^o$, and stops being effective at $\delta_f > 30^o$ for the same reason as the aft slot. The FWD slot is exposed to the external flow only for $\delta_f > 22^o$ and becomes effective only for $\delta_f > 30^o$, peaks at $\delta_f \approx 50^o$, and losses effectiveness at $\delta_f \approx 60^o$. The effective range of each slot versus δ_f is not significantly sensitive to the $< c_\mu >$ or F^+ (using $F^+ > 4$), as shown by the data (Fig. 6) for $Re_c = 0.75x10^6$ using the FWD slot, acquired at a lower Re_c and F^+ than the Re_c=0.41 x 10^6 for the FWD slot. A small adverse effect at the edges of the effective range of each slot is also shown in Figure 6. Such effects were not seen when using low F^+ excitation or LE excitation, and the source for the current effect is unknown. Note that the small difference in slot locations ($\Delta x/c \approx$3.2%, Fig. 1(b) and Table 1) between the FWD slot and slot #3, results in a 30^o change in δ_f for max effectiveness of the two slots, while the difference between the aft slot and slot #3 ($\Delta x/c \approx$9%) results in only a 3-4^o difference in δ_f for maximum effectiveness. A possible explanation for this significant finding is the curvature in the FWD slot region, while the the upper flap surface, downstream of slot #3, is almost flat.

3.3 TE Flap FWD Slot AFC Results

Figure 7(a) shows the lift increment and form–drag alteration due to high F^+, pure sine excitation and amplitude modulation of the F^+=13 excitation at F^+_{AM}=0.32 (Note curve fitted data). The choice of this F^+_{AM} will be explained later. It clearly shows that larger lift increments are generated between $30^o < \delta_f < 50^o$ when using $F^+_{AM} = 0.32$ rather than only $F^+ = 13$, while the high F^+ excitation reduces the form drag more effectively throughout the δ_f range. The data further indicates that the longer wave length generated by the $F^+_{AM} = 0.32$ excitation is less sensitive to the curvature of the flap surface, reducing the effective δ_f range of the FWD flap slot by about 10 degrees, with respect to the pure sine, high frequency excitation. The application aspect of the above finding is that it should be possible, by only changing the excitation frequency, to alter the lift to drag ratio, while maintaining lift and to obtain similar effects as would be obtained by altering the excitation slot location. These effects presumably are related to the relationship between the convective low F^+ AM wave length with regard to the radius of curvature at the slot region.

The increase in form drag when using the F^+_{AM} excitation may be due to exciting the flow near the natural vortex shedding frequency. It was recently shown (Naim et al,[13] Naim [14]) that excitation at frequencies close to the natural vortex shedding frequency (VSF) increases the drag of bluff bodies. This occurs due to closer forming and more energetic Karman vortices in the wake of the separated bluff body. The combined effect induces a stronger upstream directed flow (in a frame of reference advected with the body), hence larger drag. It remains to be seen if a similar mechanism is active in separated flow over conventional airfoils as well. The natural VSF of the base flow data described in Fig. 7(b) and Fig. 7(c) can be deduced from the pressure spectra measured at the trailing edge shown in Fig. 7(d). The data show a distinct peak at $F^+ \approx 0.3$.

The C_p distributions and wake profiles at δ_f=45^o are presented in Figs. 7(b)-7(c) and provide a possible explanation for the effects of the excitation on the C_L and C_{dp}. The low F^+ excitation generates mostly an upstream effect, that is crucial for the lift increment at high δ_f's. The larger C_p on the TE flap generated by the high F^+, pure sine wave, excitation is beneficial for drag reduction (Fig. 7(c)) due to the larger pressure on the negatively sloped TE flap upper surface indicated by the narrower wake and the slightly higher VSF (Fig. 7(d) $F^+ = 13$). The modification of the C_p upstream of the excitation slot, without a downstream effect on the TE flap C_p could not be explained based on the available data and it could only be speculated that a modification of the wake could produce this upstream effect. There might be two competing mechanisms at work when the complex AM excitation signal is applied. The high frequency content causes the flow to effectively turn around the flap shoulder, in a manner similar to ideal corner flow, accelerating and generating a pressure suction peak. The low F^+ content due to the AM signal, on the other hand, locks the VSF to the AM excitation frequency through a non linear process, widening the wake and increasing the pressure on the separated flap. This hypothesized mechanism requires further study. From the avail-

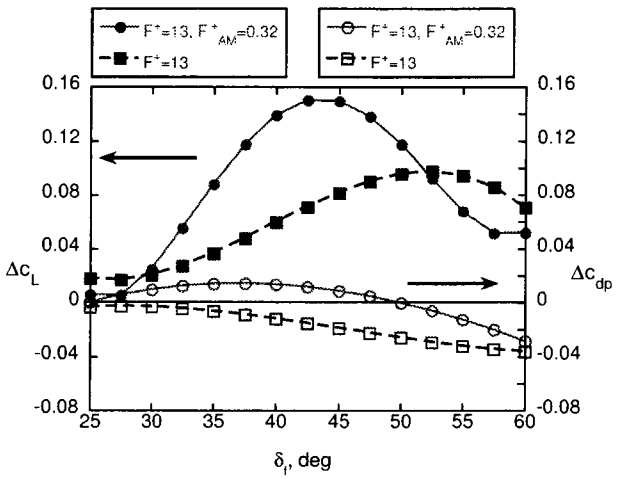

a) ΔC_L and ΔC_{dp} as a function δ_f

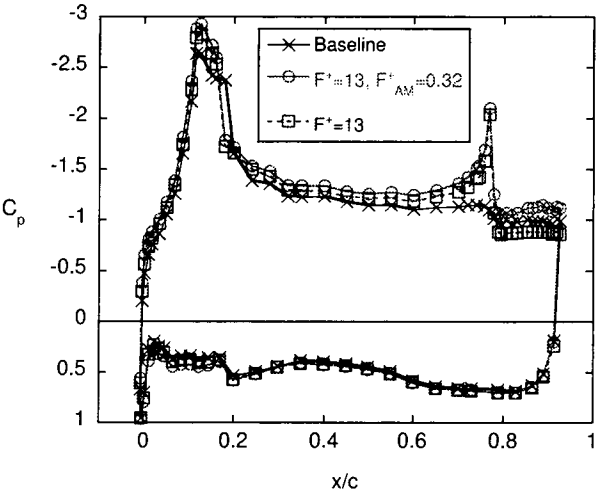

b) Pressure Distribution, $\delta_f = 45^o$

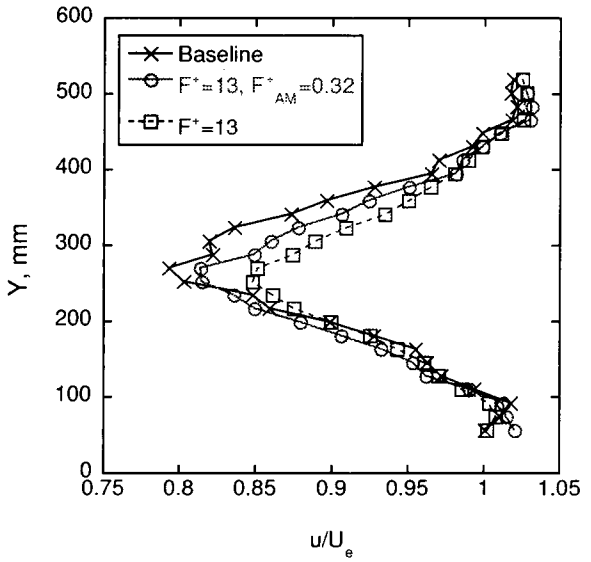

c) Wake distribution, $\delta_f = 45^o$

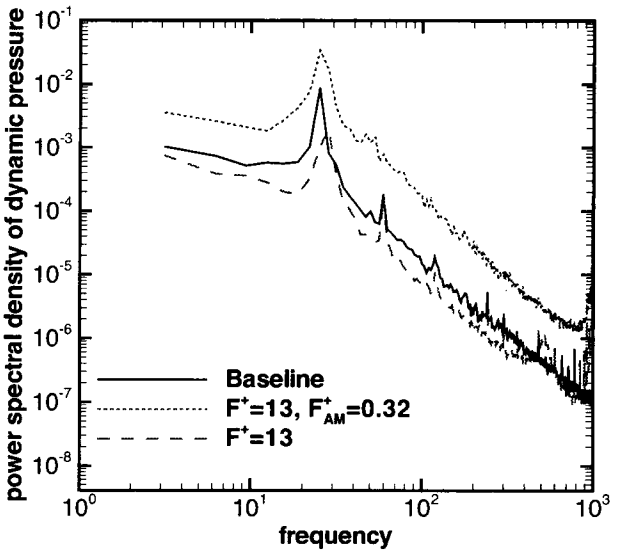

d) Flap trailing edge pressure spectra, $\delta_f = 45^o$

Fig. 7 FWD Flap Slot Control. Re_c**=0.24x10**^{6}, $\alpha = 0^o, \delta_s = -25^o, < c_\mu >$**=0.55%**

able data it seems that the high F^+ excitation delays separation, narrows the wake, increases the VSF and reduces form drag (Figs. 7(b), 7(c), and 7(d)). The AM excitation increases the magnitude of the VSF (Fig. 7(d) closer and stronger vortices), that is now the AM F^+ and increases the form drag (Fig. 7(a)). Note that the total drag, predicted from the wake momentum deficit for the AM data is less reliable due to the low frequency oscillation of the wake flow, as indicated by the TE pressure spectra (Fig. 7(d)).

3.4 TE Flap Slot #3 AFC Results

The lift increment versus flap deflection angle for excitation emanating from slot #3 at $Re_c = 0.24x10^6$ and $0.41x10^6$ is presented in Fig. 8. The values of F^+ are 12 and 7 and the values of $< c_\mu >$ are 3% and 1% for the low and high Re_c's, respectively. The data shown in Fig. 8 indicate that Re_c has a weak effect on the optimal δ_f of slot #3 excitation and that for triple the value of $< c_\mu >$, only twice the lift increment is obtainable at the lower Re_c. In Fig. 9, the effect of airfoil angle of attack on optimal δ_f for slot#3 is examined at $Re_c = 0.24x10^6$. The data indicate that airfoil α has no effect on the optimal flap deflection or on the attainable lift increment when using slot #3 with $\delta_s = -25^o$. This finding is encouraging when attempting to increase $C_{L,max}$.

3.4.1 The Effect of Low F^+ AM Excitation

As already seen in Fig. 7, low frequency modulation of the high F^+ excitation increases the lift generating capability of the flap flow forcing mechanism, while generally increasing rather than decreasing the form drag. Detailed AM frequency scans are presented and

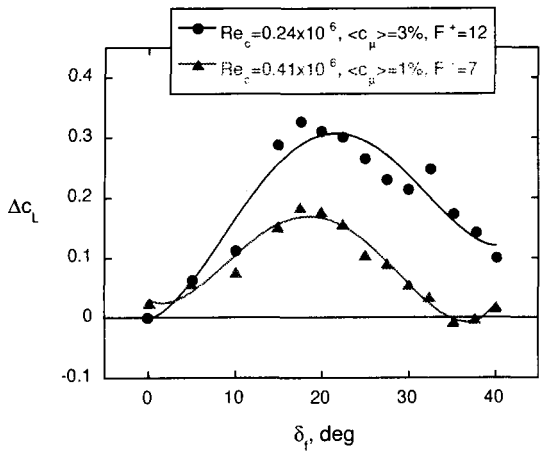

Fig. 8 Reynolds number effect on lift increment vs. flap deflection angle, $\alpha = 0^o$, $\delta_s = -25^o$, flap slot #3.

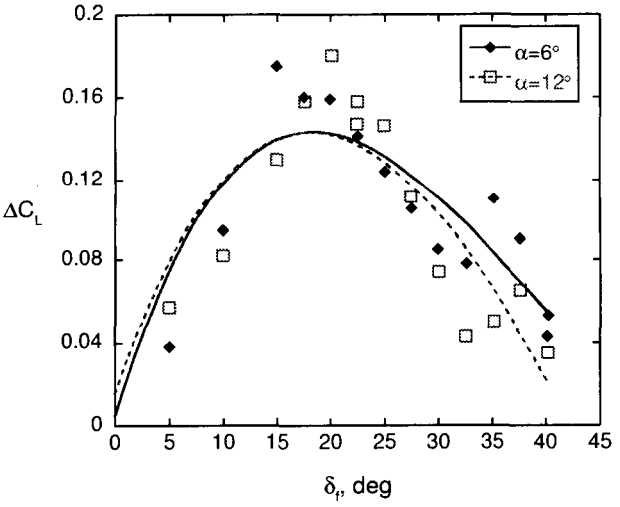

Fig. 9 Angle of Attack effect on lift increment vs flap deflection angle, $Re_c = 0.24x10^6$, $\delta_s = -25^o$, flap slot #3.

discussed in this section.

Figure 10 shows the effect of variations in the F^+_{AM} on the lift and form drag with excitation introduced from slot #3, ($\alpha = 0^o$, $\delta_s = -25^o$, $\delta_f = 20^o$, and $Re_c = 0.24x10^6$), using $< c_{\mu,AM} > = 0.6\%$. The AM data is compared to pure sine, high F^+, high $< c_\mu >$ (1.8%) data (plotted as square symbols at F^+_{AM}=0). Note that triple the $< c_\mu >$ using pure sine excitation generates approximately the same variation in lift and form drag as the optimal F^+_{AM}. Also, the optimal values of F^+_{AM} are different for the lift increment (without form–drag reduction) and form–drag reduction (at half the $\Delta C_{L,max}$). The optimal reduced AM frequencies are $F^+_{AM} \approx 0.5$ for lift increment and $F^+_{AM} \approx 1$ for form-drag reduction. The F^+ sensitivity data are consistent with the pure harmonic low frequency scan performed by Seifert et. al[1] for lift increment purposes, and the form–drag reduction found at twice the optimal ΔC_L frequency was also seen by Naim.[13,14]

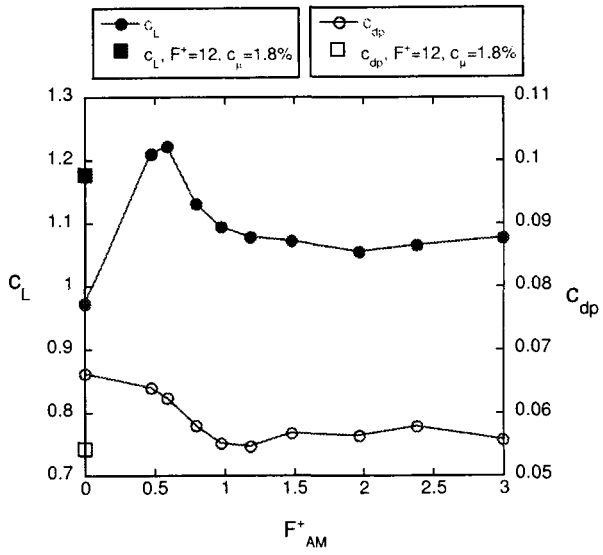

Fig. 10 Effect of F^+_{AM} on C_L and C_{dp}, $\alpha = 0^o$, $\delta_s = -25^o$, $\delta_f = 20^o$, flap slot #3 (see fig. 1(b). $Re_c = 0.24x10^6$, $< c_\mu >$=0.6%.

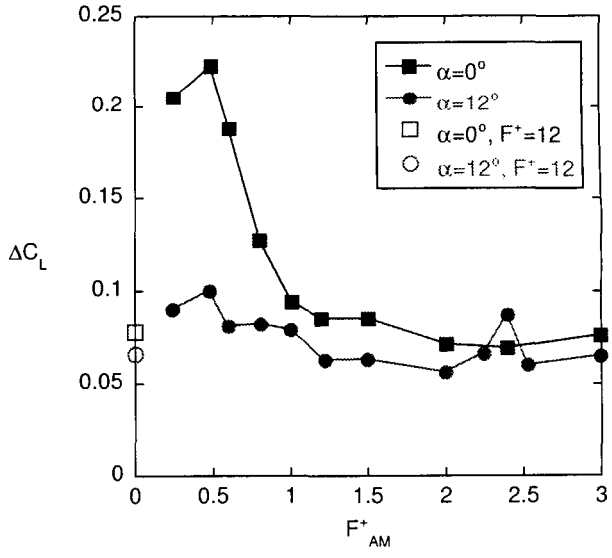

Fig. 11 F^+_{AM} Effect, $Re_c = 0.24x10^6$, $\delta_f = 20^o$, $\delta_s = -25^o$, Flap slot #3, $< c_\mu >$=0.6%.

Figure 11 compares the lift increment at $\alpha = 0^o$ and $\alpha = 12^o$ ($C_{L.max}$) with excitation introduced from slot #3. The data indicate, in agreement with Seifert and Pack,[2] that the lift increment is approximately halved (using the same $< c_\mu >$) when approaching $C_{L.max}$, but the effective F^+_{AM} remains unchanged. The lift increment reduction is attributed to the boundary layer thickness increase, larger adverse pressure gradient on the TE flap, the intermittently separated flow, and the slot location.

Figure 12(a) shows the lift increment and Fig. 12(b) shows the form–drag variations, comparing magnitude effect of pure sine, high frequency excitation to those

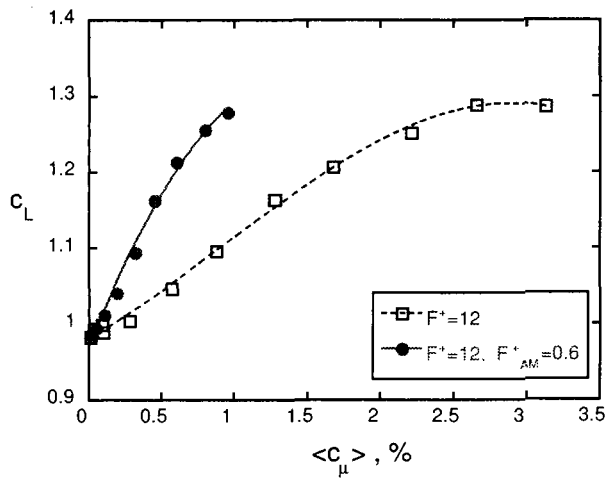

a) $< c_\mu >$ **effect on** C_L

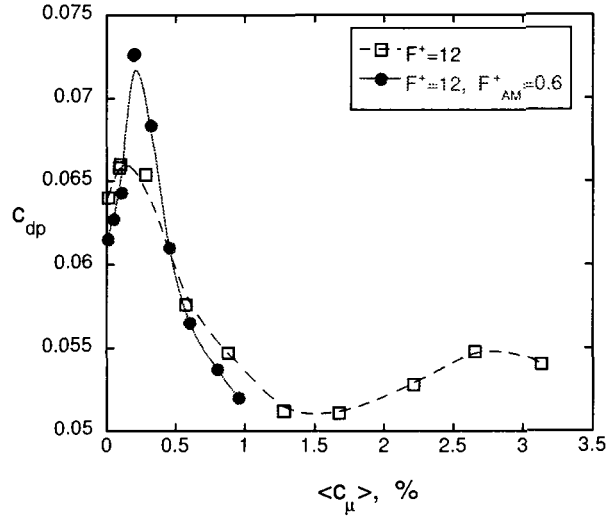

b) $< c_\mu >$ **effect on** C_{dp}

Fig. 12 Amplitude Scan. Flap slot #3, $Re_c = 0.24x10^6$, $\delta_s = -25^o$, $\delta_f = 20^o, \alpha = 0^o$.

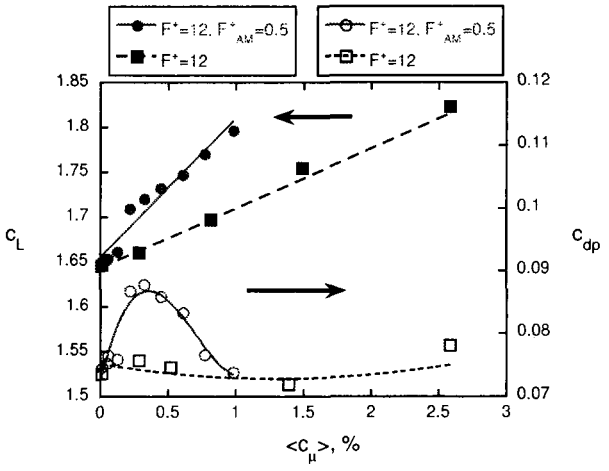

a) **Effect of Pure Sine control and AM control on** C_L **and** C_{dp}.

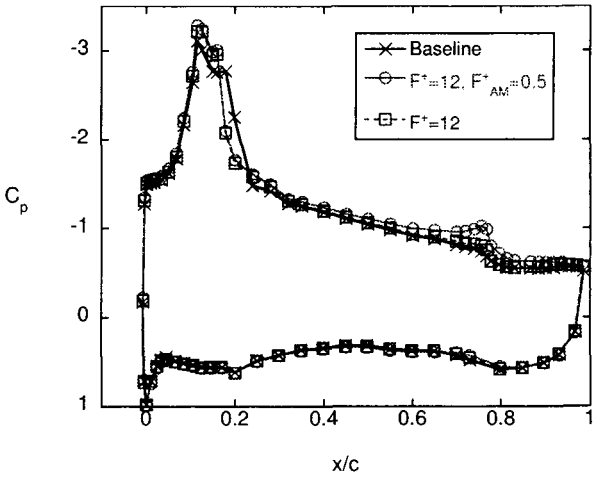

b) C_p **plot at** $< c_\mu >$**=0.3%**

Fig. 13 Amplitude Scan. Flap slot #3, $Re_c = 0.24x10^6$, $\alpha = 6^o$, $\delta_s = -25^o$, $\delta_f = 30^o, \alpha = 0^o$.

due to F^+_{AM}=0.6 excitation. The results indicate that only a third of the $< c_\mu >$ is required to generate the same increment in lift when using $F^+_{AM} = 0.6$. The form drag (Fig. 12(b)) initially increases for low levels of $< c_\mu >$ (more significantly for $F^+_{AM} = 0.6$); however, for $< c_\mu >$>>0.5% the trend of the drag data is similar, regardless of the excitation signal frequency content.

Figure 13(a) shows data similar to that of Fig. 12(a), but at a larger incidence angle of $\alpha = 6^o$. The low F^+_{AM} is still more energy efficient, but the form drag is not increased by using high frequency excitation. It requires, again, roughly 33% $< c_\mu >$ to generate the same ΔC_L, while drag is not reduced by the available range of $< c_\mu >$. The low F^+_{AM} excitation still shows a stronger upstream effect (Fig. 13(b)), increasing *both* C_L and C_{dp}.

3.5 Flow Details and Separation Detection Criteria

To better explore flow modifications due to the excitation and correlate these to variations in the separation location and eventually to alternation of the aerodynamic performance of the wing in the high lift configuration, flow physics details need to be studied and understood. For this purpose C_p, hot-film and dynamic pressure data are correlated with flow field data acquired by DPIV, as described in Section 2, and will be discussed in this section.

Figure 14(a) shows the C_p distributions of the baseline and F^+=12 controlled flow fields at $\alpha = 6^o$. The excitation is introduced from slot #3 indicated by the vertical, dotted line at x/c=0.78. A strong suction peak was established at the slot and upstream acceleration was induced due to the excitation. The flow on the TE flap is partially reattached resulting in a ΔC_L=0.17 and ΔC_{dp}=0.004 (excitation increases both

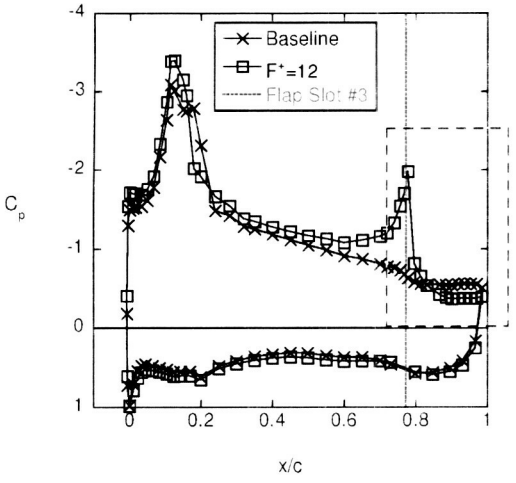

a) C_p distribution

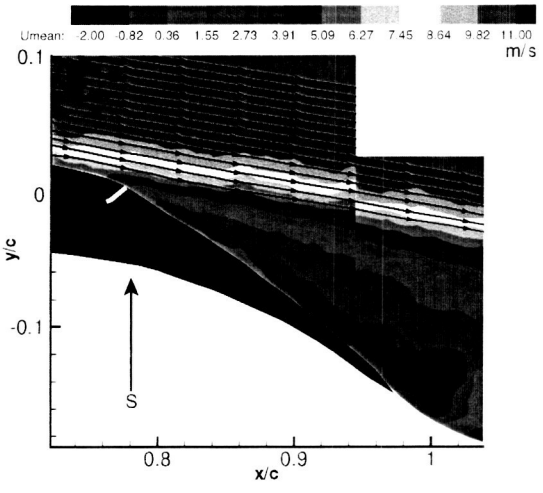

b) PIV Baseline

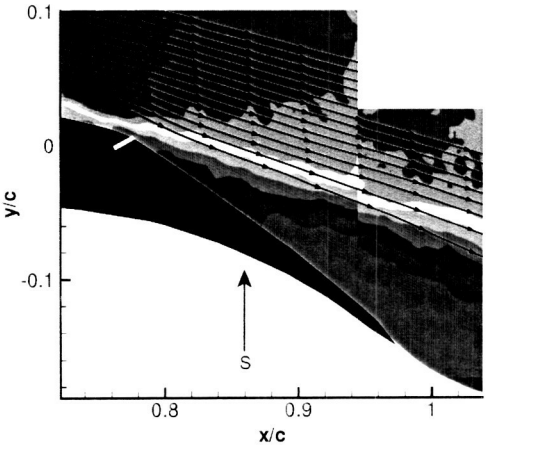

c) PIV Controlled, F^+=12, $< c_\mu >$=2.5%

Fig. 14 Baseline and controlled flow field. $Re_c = 0.24x10^6$, $\alpha = 6^o$, $\delta_s = -25^o$, $\delta_f = 20^o$, F^+=12, $< c_\mu >$=2.5%.

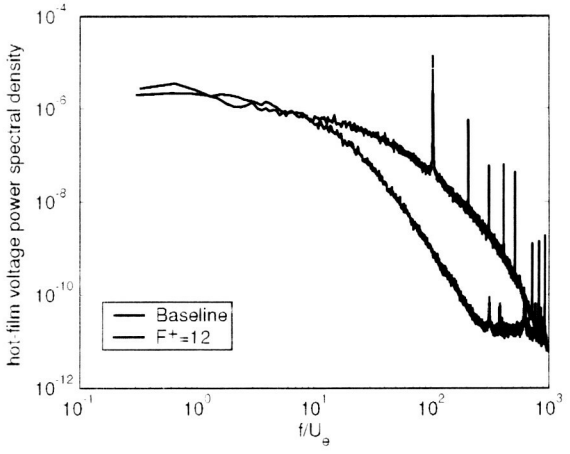

Fig. 15 Spectra at x/c=0.081, $\alpha = 6^o$, $\delta_s = -25^o$, $\delta_f = 20^o$, **flap slot #3 (see fig. 1(b).** $Re_c = 0.24x10^6$, $< c_\mu >$=2.5%

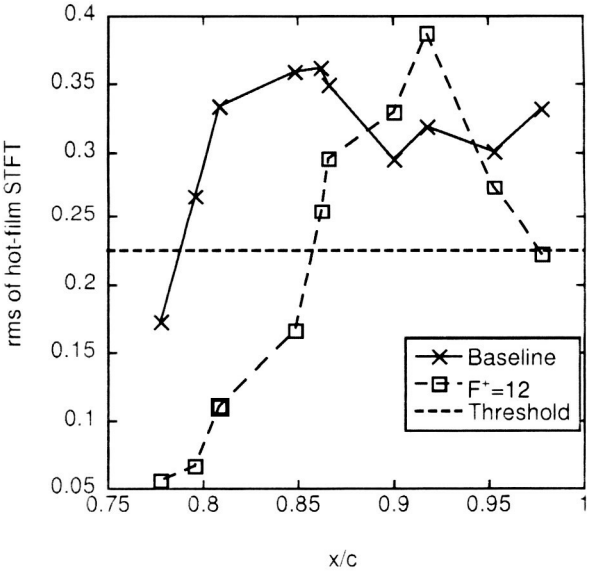

Fig. 16 TE Flap hot-film stft rms, $\alpha = 6^o$, $\delta_s = -25^o$, $\delta_f = 20^o$, **flap slot #3 (see fig. 1(b).** $Re_c = 0.24x10^6$, $< c_\mu >$=2.5%.

C_L and C_{dp} at this condition). The excitation on the TE flap also promotes transition on the LE flap (presumably due to the increased circulation over the entire airfoil that generates a more severe adverse pressure gradient or due to an acoustic disturbance) and reduces the length of the separation bubble seen at x/c=0.20 in the baseline C_p distribution (Fig. 14(a)). The dashed box in Figure 14(a) represents the region where the PIV data was acquired and these data are presented in Fig. 14(b)-14(c). The PIV data, acquired using two cameras, shows that the baseline flow separates from the TE flap at x/c $\approx$ 0.8 (Fig. 14(b)- 14(c)) and the separated streamline flows at an angle of -10^o with respect to the freestream. When excitation from slot #3 is introduced, separation is delayed to x/c$\approx$0.9

and the separating streamline angle is -23^o, while inclination of the upper surface of the TE flap is about -36^o. The induced upstream acceleration can be seen by the reduction in δ^* at x/c=0.74 from 6.1 mm in the baseline to 3.3 mm in the controlled flow.

In Ref. 8, the Short Time Fourier Transform (STFT) of the hot-film signals was used to determinine the separation location. Separation is an intermittent process in that at a point on the surface in the vicinity of separation there would be a lower probability of encountering small scale structures affecting the hot-film signal as separation develops. The result of this process on the dynamics can be seen when one compares spectra between separated and attached flow. For the separated flow there is a loss of high frequency energy as shown in Fig. 15. However, with the STFT the time scale of the loss of energy at high frequencies is more evident, since the process is highly non-stationary in nature. This qualitative analysis of the flow is a good indication of the state of the boundary layer but a way to quantify this result is needed. It is proposed that the an rms-like value can be used to quantify the STFT results. The STFT rms quantity is determined using the following steps.

I) The STFT is computed using the voltage from each hot-film sensor. The window length for the STFT is 40 ms and 5 sec of data are sampled at 25.6 kHz.

II) A comparison of spectra in attached and separated flow regions indicates that the loss of energy occurs above f/U_e=5, where U_e is the boundary layer edge velocity computed using the C_p distribution.

III) The equation below is evaluated

$$FFTm(t) = \int_{5.0U_e}^{7000} |FFT(f)|\, df \qquad (1)$$

in order to determine the power in the spectra above the cut off frequency, $5.0 * U_e$. This is repeated for each 40 msec window of the STFT at each hot-film location.

IV) The STFT rms is the standard deviation of $FFTm(t)/mean(FFTm(t))$.

The STFT rms data shown in Fig. 16, using a threshold level of 0.225, indicate separation occurs in the same region shown by the C_p distribution and PIV data, in Figures 14(a)-14(c) .

3.6 Combination of LE and TE Control

To effectively use the potential of the high lift system, separation should be controlled on both the LE and TE flap shoulders. The role of the LE actuator would be to maintain mostly attached flow on the entire main element, resulting in attached flow at the TE flap slot location. Otherwise separation would take place upstream of the active slot, voiding its effectiveness, that relies on mixing enhancement. If the separated shear layer is remote from the active slot, communicated only by dead air, high momentum fluid can not be transported to the vicinity of the flap and its effectiveness would be low. While Reference 8 described the application of AFC to the LE flap shoulder with the aim of maintaining attached flow on the main element up to $C_{L,max}$, the majority of the current paper was devoted to AFC application on the TE flap upper surface. Effects attributed to curvature, increased BL thickness and larger adverse pressure gradients are significantly complicating AFC application at the TE flap region. Nonetheless, combined LE and TE flap AFC was attempted at low flap deflections where AFC benefits on the flap performance persisted to $C_{L,max}$.

Figure 17 shows preliminary data combining the LE actuator with the TE flap actuator. The data presented are at $Re_c = 0.41x10^6$ with $\delta_f = 5^o$ and $\delta_s = -25^o$. Excitation at the LE flap shoulder alone using F^+=22 is compared to excitation using F^+=22 with F^+_{AM}=4, showing slightly superior results due to the AM excitation. The TE flap actuator was operated at F^+=5 and excitation was introduced through the AFT slot. In this case, $< c_\mu >$ for the TE flap and LE flap actuators was 0.35% and 0.015%, respectively. Excitation at the LE flap shoulder (x/c=0.14%) using either the pure sine signal or the AM signal, increased $C_{L,max}$ by 0.05 and delayed stall by 2^o. Control applied from the AFT slot of the flap alone increased lift at stall by 0.03, but did not alter the stall angle. Note that typically increasing flap effectiveness or loading causes earlier flap stall. When the LE and TE excitations were combined, it resulted in similar gains in performance until $\alpha = 14^o$, where $C_{L,max,bas}$ was measured, but the combination of pure sine, high frequency excitation was more effective at larger α, increasing $C_{L,max}$ to 2.1 and delaying stall to 16^o. The larger effect of the high frequency LE excitation combined with the TE excitation might be connected to the absence of large coherent structures generated by the low frequency AM excitation, causing intermittently reversed flow at the the flap shoulder location.

4 Summary and Conclusions

Although flow separation from the leading edge could be controlled using relatively low $< c_\mu >$ excitation, controlling separation on the trailing edge flap requires larger periodic momentum input. As was the case when controlling separation at the leading edge, AM of the high frequency excitation reduced the required $< c_\mu >$. While a 50% reduction in $< c_\mu >$ was seen when using AM excitation at the leading edge, a factor of 3 reduction in $< c_\mu >$ was measured when using AM on the trailing edge flap.

Curvature is believed to play an important role in

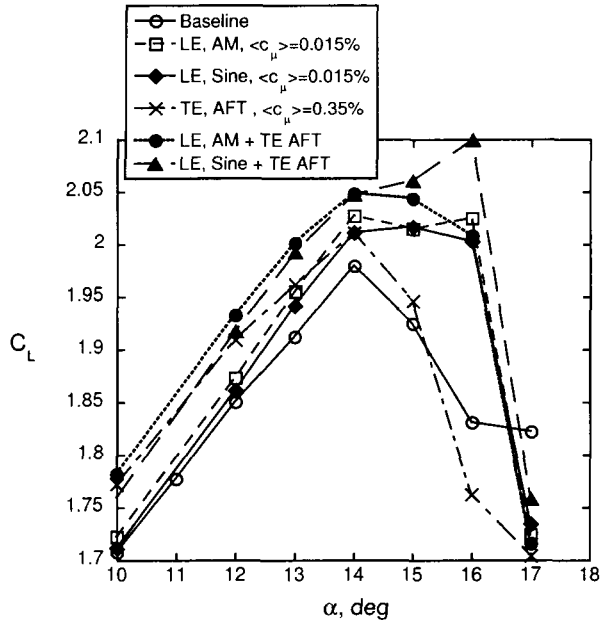

Fig. 17 Effect of LE and TE flap control on C_L. $Re_c = 0.41x10^6$, $\delta_f = 5^o$, $\delta_s = -25^o$, F^+_{LE}=**22**, $F^+_{AM,LE}$=**4**, F^+_{flp}=**5**.

the separation control process and the ratio between the resulting excitation wavelength and the radius of curvature might be a relevant parameter. The optimal trailing edge flap defection for a particular excitation slot location on the trailing edge flap changed significantly in regions of high curvature. Near the shoulder of the trailing edge flap, where the surface is highly curved, a Δx/c of 3.2% caused a 30^o change in the δ_f for maximum effectiveness. While in a region where the TE flap was not highly curved, a Δx/c of 9% caused only a 3-4^o change in δ_f for maximum effectiveness.

The combination of LE and TE excitation is the primary goal of the research. Preliminary data using combined LE and TE excitation indicates that increased airfoil performance can be obtained when control applied simultaneously at both locations. LE control with AM excitation was more effective than high frequency pure sine excitation when using the same $< c_\mu >$. However, when high frequency pure sine excitation at the TE flap was combined with the LE excitation, better performance gains were measured when using high frequency pure sine excitation at the leading edge. Additional data will be acquired in an upcoming test of the same model with both excitations active. In addition, the airfoil performance with the actuator upstream of the TE flap will be evaluated.

5 Acknowledgements

The authors would like to thank the following individuals for their support of the research program, Anna McGowan, William Sellers, Michael Walsh, Anthony Washburn, Luther Jenkins, John Lin, Norman Schaeffler, Richard White, George Hilton, Johnny Mau, Louis Hartzheim, Susan Palmer, and R. David Lewis.

References

[1]Seifert, A., Darabi, A., and Wygnanski, I., "On the Delay of Airfoil Stall by Periodic Excitation," *Journal of Aircraft*, Vol. 33, No. 4, 1996, pp. 691–699.

[2]Seifert, A. and Pack, L. G., "Oscillatory Control of Separation at High Reynolds Numbers," *AIAA Journal*, Vol. 37, No. 9, 1999, pp. 1062–1071.

[3]Seifert, A. and Pack, L. G., "Active Flow Separation Control on Wall-Mounted Hump at High Reynolds Numbers," *AIAA Journal*, Vol. 40, No. 7, 2002, pp. 1363–1372.

[4]McClean, J. D., Crouch, J. D., Stoner, R. C., Sakurai, S., Feifel, G. E., Feifel, W. M., and Rush, H. M., "Study of the Application of Separation Control by Unsteady Excitation to Civil Transport Aircraft," NASA/CR 1999–209338, 1999.

[5]Lin, J. C. and Dominik, C. J., "Parametric Investigation of a High-Lift Airfoil at High Reynolds Numbers," *Journal of Aircraft*, Vol. 34, No. 4, 1997, pp. 485–491.

[6]G.V.Lachmann, *Boundary Layer and Flow Control, Vol. 1*, Pergamon Press Inc., 1961.

[7]Margalit, S., Greenblatt, D., Seifert, A., and Wygnanski, I., "Active Flow Control of a Delta Wing at High Incidence using Segmented Piezoelectric Actuators," AIAA Paper 2002–3270, June 2002.

[8]Pack, L. G., Schaeffler, N. W., Yao, C., and Seifert, A., "Active Control of Separation from the Slat Shoulder of a Supercritical Airfoil," AIAA Paper 2002–3156, June 2002.

[9]Lin, J. C., "Unpublished EET data," Private communication.

[10]Barlow, J. B., W. H. Rae, J., and Pope, A., *Low Speed Wind Tunnel Testing*, John Wiley and Son, 1999.

[11]Abbott, I. H. and van Doenhoff, A., *Theory of Wing Sections*, Dover Publications, 1949.

[12]Hoerner, S. F. and Borst, H., *Fluid-Dynamic Lift: Practical Information on Aerodynamic and Hydrodynamic Lift*, Hoerner Fluid Dynamics, 1975.

[13]Naim, A., Greenblatt, D., Seifert, A., and Wygnanski, I., "Active Control of Cylinder Flow with and without a Splitter Plate using Piezoelectric Actuators," AIAA Paper 2002–3070, June 2002.

[14]Naim, A., *Active Control of Cylinder Flow with and without a Splitter Plate*, Master's thesis, Dep. of Fluid Mech. and Heat Transfer, Faculty of Engineering, Tel-Aviv University, Israel, March 2003.